FEBS Letters 587 (2013) 339–344

FEBS Letters

journal homepage: www.FEBSLetters.org

The crystal structure of the cysteine protease Xylellain from *Xylella fastidiosa* reveals an intriguing activation mechanism

Ney Ribeiro Leite [a,1,2], Aline Regis Faro [a,1,3], Maria Amélia Oliva Dotta [a], Livia Maria Faim [a], Andreia Gianotti [b], Flavio Henrique Silva [b], Glaucius Oliva [a], Otavio Henrique Thiemann [a,*]

[a] *Instituto de Física de São Carlos, Universidade de São Paulo, São Carlos, SP 13566-590, Brazil*
[b] *Department of Genetics and Evolution, Federal University of São Carlos, São Carlos, SP 13565-905, Brazil*

ARTICLE INFO

Article history:
Received 11 September 2012
Revised 21 December 2012
Accepted 3 January 2013
Available online 17 January 2013

Edited by Stuart Ferguson

Keywords:
Cysteine protease
Xylellain
Crystal structure
Xylella fastidiosa

ABSTRACT

***Xylella fastidiosa* is responsible for a wide range of economically important plant diseases. We report here the crystal structure and kinetic data of Xylellain, the first cysteine protease characterized from the genome of the pathogenic *X. fastidiosa* strain 9a5c. Xylellain has a papain-family fold, and part of the N-terminal sequence blocks the enzyme active site, thereby mediating protein activity. One novel feature identified in the structure is the presence of a ribonucleotide bound outside the active site. We show that this ribonucleotide plays an important regulatory role in Xylellain enzyme kinetics, possibly functioning as a physiological mediator.**

Structured summary of protein interactions:
Xylellain and **Xylellain** bind by X-ray crystallography (View interaction)

© 2013 Federation of European Biochemical Societies. Published by Elsevier B.V. All rights reserved.

1. Introduction

Xylella fastidiosa is a gram-negative bacteria that colonizes exclusively the plant xylem vessels decreasing xylem flow compromising the plant development and are difficult (*fastidious*) to culture by standard bacteriological procedures [1–3]. Several economically important crops are affected by *X. fastidiosa* strains [4–8] that are transmitted by Homoptera (leafhoppers) insects [9,10]. In Brazil alone, citrus variegated chlorosis or CVC cause approximate annual losses to the citrus industry of US $100 million [11] whose control is limited to crop management, infected branches pruning and plant eradication. The use of healthy seedlings and vector control are at present the only preventive measures available. The availability in 2000 of the *X. fastidiosa* clone 9a5c genome sequence [12] lead to a significant advance in the understanding of the bacterium metabolism [2,3]. From *X. fastidiosa* genome analysis a single cysteine protease was identified, Xylellain, and characterized as a cathepsin B like protease [13]. In this study, we solved the crystal structure of Xylellain, to a resolution of 1.65 Å. This structure revealed that the first 39 residues of the enzyme N-terminal sequence are attached to the active site and represent a regulatory pro-region. Surprisingly a ribonuclotide, UDP, is present in a hinge region and may play an important role in stabilizing the N-terminal pro-region, representing a potential enzyme activity modulator, sensing the bacteria physiological state.

2. Materials and methods

2.1. Recombinant Xylellain characterization

The expression and purification of the recombinant Xylellain protein was performed essentially as previously described [13] modified by the induction temperature reduced to 20 °C for 16 h and isopropyl-b-D-thiogalactopyranoside (IPTG) added to a final concentration of 0.1 mM selenomethionine incorporation for single-wavelength anomalous dispersion (SAD) experiments was performed by inhibition of methionine biosynthesis in M9 minimal medium (Sigma) supplemented by selenomethionine (Sigma) [14].

Point mutations R23A, F25A and R23A/F25A, were generated using the Gene Tailor™ Site-Directed Mutagenesis kit (Invitrogen), according to the manufacturer's instructions and the oligonucleotides: R23A, 5′-ATAGCTGATATTGCTGACTTTTCATACACC-3′; F25A, 5′-GATATTCGTGACGCTTCATACACCCCAGAG-3′; R23A/F25A, 5′-ATAGCTGATATTGCTGACGCTTCATACACCCC-3′ and their complementary primer: R23A and R23A/F25A, 5′-ATAGGGTCTATATCGAC-

* Corresponding author. Fax: +55 1633739881.
E-mail address: thiemann@ifsc.usp.br (O.H. Thiemann).
[1] Both authors contributed equally to this work.
[2] Present address: Cristália Produtos Químicos Farmacêuticos Ltda. Rodovia Itapira-Lindóia, km 14, Itapira, SP, Brazil.
[3] Present address: Institut de Biologie Structurale Jean-Pierre Ebel, Université Joseph Fourier, 41 rue Jules Horowitz, F-38027 Grenoble, France.

0014-5793/$36.00 © 2013 Federation of European Biochemical Societies. Published by Elsevier B.V. All rights reserved.
http://dx.doi.org/10.1016/j.febslet.2013.01.009

TATAA-3′, F25A, 5′-TCTATATCGACTATAAGCACTG-3′. Mutant Xylellain proteins were expressed and purified as described.

Enzyme kinetic experiments were performed as described [13] in a WALLAC 1420 fluorimeter using carbobenzoxy-Phe-Arg-7-amido-4-methylcoumarin (Z-RF-MCA, Sigma) as substrate. The amount of active enzyme was determined by titration with E64 (N-[N-(L-3-trans-carboxyoxirane-2-carbonyl)-L-leucyl]-agmatine) inhibitor [15].

2.2. Crystallization and data collection

Suitable crystals were obtained at 18 °C using the hanging-drop vapor diffusion technique in 60 mM sodium citrate (pH 5.6), 134 mM ammonium acetate and 20–22% (w/v) PEG 4000 and 7 mg/ml of Xylellain. The crystals were cryoprotected in the crystallization solution containing 15% (v/v) ethylene glycol and frozen to 100 K. A native data set was collected to 1.65 Å resolution, on a MAR345dtb image-plate detector using Cu Kα radiation generated by a Rigaku Ultra-X 18 rotating-anode operating at 90 mA and 50 kV and focused using Osmic mirrors. Selenomethionine crystals were obtained by the hanging-drop vapor diffusion method in 100 mM MES (pH 5.6), 18% PEG 8000 and 6 mg/ml of Xylellain. Selenomethionine data sets were collected at the National Synchrotron Light Source, Brookhaven National Laboratory, Beamline X12B. Xylellain diffraction data for the Sel-Met crystal were indexed, integrated and reduced using HKL2000 package [16] while for the native crystal, the data processing was carried out using MOSFLM [17]. Intensities were scaled with SCALA from the CCP4 suite [18]. Data collection and processing statistics are provided in Table 1. Both native and selenomethionine crystals belong to space group P1 with similar cell dimensions and Matthew's coefficient [19] calculated to 2.16 $Å^3$/Da with a solvent content of 43.02%.

2.3. Structure solution and refinement

Searches on the PDB database identified *Cathepsin S* and *F* [20,21] and *Cruzain* [22] as Xylellain homologues with 30% sequence identity. Molecular replacement attempts to solve the Xylellain structure with AmoRe [23], MOLREP [24] and PHASER [25] were not successful justifying the use of selenomethionine isomorphous replacement methodology.

The selenomethionine Xylellain structure was solved by SAD method at the Se-K edge (λ = 0.9792). Eight selenium atoms per cell unit were found using SHELX package [26], initial phases were obtained with SOLVE [27] and improved by solvent flattening and density modification with 42% solvent content, followed by auto building routine with RESOLVE [28]. Residues of the initial model were checked according to their electronic density with COOT [29]. Initial phases were extended with sequential rounds of solvent flattening and density modification using the selenomethionine-containing and native data sets. Cycles of SOLVE–RESOLVE routine successfully traced and built 665 residues of the expected 1164, with an R_{factor} 43% and merit figure of 0.55. The remaining model was built manually with COOT followed by refinement with REFMAC [18]. Water molecules were added by COOT and the structure was validated using PROCHECK [30]. All pictures were created using PyMOL [31].

3. Results

3.1. Crystalline packing and overall structure

Both the selenomethionine and the native Xylellain crystals belong to the P1 space group, with similar unit cell parameters, containing four Xylellain monomers (chains A–D) (Fig. 1). A contact surface of 2018 $Å^2$ between chains A/B and C/D is stabilized by polar contacts involving a minimum of 19 residues of each monomer, 13 hydrogen bonds and 6 salt bridges. In this crystal packing the active site and the propeptide domain belong to the dimer interface in the A/B and C/D chains. The atomic contacts between chains A/B with C/D is characterized by fewer interactions.

The adopted residue numbering initiates at Met1 from Xylellain full length sequence (GenBank accession No. AE003869, locus_tag XF_0156, complement of position 159327–160142). Final refinement shows 1435 waters molecules and a ribonucleotide (UDP) molecule at each chain.

The first 22 and 23 N-terminal amino acid residues of chains A–D and B–C, respectively, representing the pET28a-derived sequence that include the hexahistidine-tag and thrombine site,

Table 1
Crystallographic data collection and refinement statistics.

Data set	Native	SelMet
Space group	*P*1	*P*1
Cell dimensions		
a, *b*, and *c* (Å)	55.089, 69.31, 82.36	55.15, 69.21, 82.27
α, β, and γ (Å)	75.86, 75.43, 66.51	76.15, 75.67, 66.64
Wavelength (Å)	1.541	0.972
Resolution (Å)	78.66–1.65 (1.74–1.65)	50.00–1.83 (1.91–1.83)
R_{merge}[a] (%)	5.4 (40.0)	5.4 (40)
I/σ (I)	9.9 (1.9)	15.1 (2.5)
Completeness (%)	91.0 (86.7)	99.5 (97.8)
Redundancy	8.1 (4.4)	4.8 (3.1)
No. of reflections observed	117070	86,291
No. of reflections unique	16,308	7651
Refinement		
Number of atoms	8578	–
R_{work}/R_{free} (%)	16.85/21.59	–
r.m.s.d.		–
Bond angles (°)	2.082	
Bond lengths (Å)	0.025	–
Ramachandran analysis (%/No.)		–
Most favored	88.7/800	
Additional allowed	10.9/98	–
General allowed	0.4/4	–

Numbers in parentheses represent the highest resolution bin.

[a] $R_{merge} = \sum_h \sum_l / I_{hl} - \langle I_h \rangle | \sum_h \sum_l \langle I_h \rangle$, where I_{hl} is the intensity of the *l*th observation of reflection *h* and $\langle I_{hl} \rangle$ are the mean intensity of the *h* reflections. R_{merge} is computed over all *l* observations of *h* reflection.

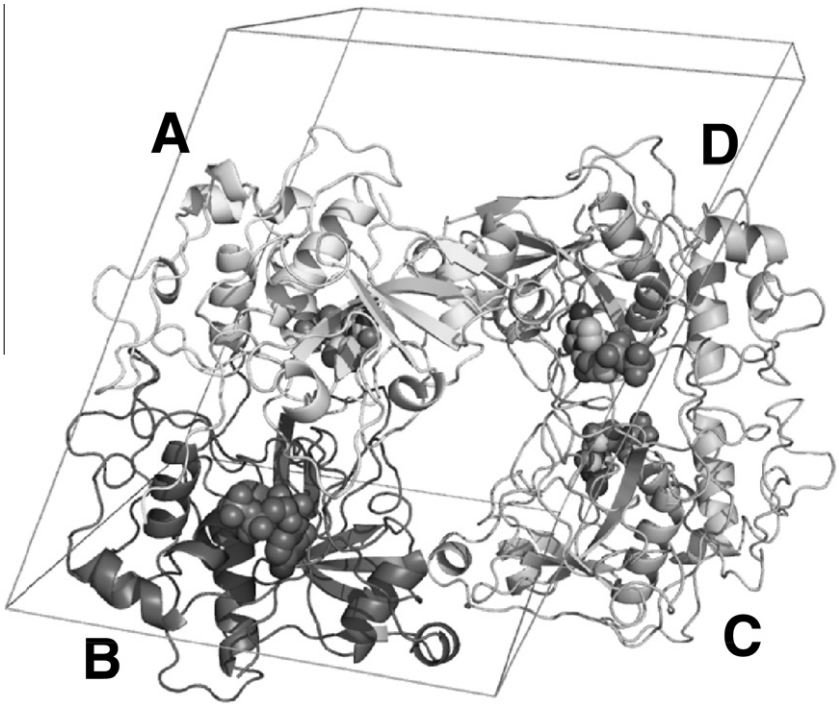

Fig. 1. Cartoon representation of the crystallographic packing of the Xylellain refined structure inside the cell unit. Each monomer, A, B, C and D of Xylellain is represented in ribbons with a diphosphate ribonucleotide in the ball-and-stick representation near the N-terminal region of each monomer.

the first two residues (MQ) of the Xylellain sequence and the last residue (Lys291) are not visible in the electron density maps. No differences were observed between the unit cell monomers as shown by the RMSD combinantion of structural superpositions 0.41 Å (AB); 0.43 Å (AC); 0.22 Å (AD); 0.29 Å (BC); 0.44 Å (BD); 0.43 Å (CD). The overall fold of Xylellain shows a core structure characteristic of the papain-like cysteine protease family [32] with a two domain arrangement, a predominantly α-helix N-terminal domain and a predominantly β-sheet C-terminal domain. The active site cleft is located at the domains interface.

3.2. The active-site cleft and N-terminal extension

The Xylellain active site is homologous to the papain family cysteine proteases, forming a cleft where the substrate peptide is fitted. The papain active site consists of seven subsites (S4, S3, S2, S1, S1′, S2′, S3′ and S4′) that interact with seven amino acids (P4, P3, P2, P1, P1′, P2′, P3′ and P4′) of the substrate peptide (Fig. 2). Xylellain active site is characterized by four residues, Gln72, Cys78, Hys237 and Asn255, where Cys78, located at the N-terminal helix α2, and Hys237 located at the strand β4 form the catalytic dyad. Gln72 precedes the catalytic (Cys78) and is responsible for the formation of the oxy-anion pocket during the peptide bond hydrolysis. Asn255, acts correctly positioning the imidazole ring of His217 through a hydrogen bond between the Nε2 of His237and Oδ1 of Gln72. The active site cleft is blocked by the N-terminal sequence (Lys29 to Ile39) analogous to other papain family cysteine proteases [33].

Xylellain structure reveals an interesting N-terminal amino acids region close to the substrate binding site. The first segment (I) of the proregion (Thr23 to Arg28) does not interact directly with the protein. While a second segment (II) of ten residues (Lys29 to Ile39) is buried within the active site cleft, between the two protein domains forming a 990 $Å^2$ surface of interaction. The two segments (I and II) are separated by two residues, Gly32 and Gly34, enabling segment I to twist approximately 70 degrees relative to segment II over the active site cleft. Segment II is stabilized by eigth hydrogen bonds (NξLys30-OSer122-3.02 Å, Nε1Trp284-Oδ2Asp38-2.83 Å; NAsp38-Oδ2Asp282-3.06 Å; *N*Ile36-*O*Ala124-2.97 Å; NεArg43-Oδ1Asp41-2.87 Å; NH1Arg43-Oδ2Asp41-2.71 Å; NH2Arg186-Oδ2Asp38-2.8 Å; NH1Arg127-OIle39-2.93 Å) and amino acids Ser31, Tyr33, Tyr35, Ile36, Asp38 side chains interact with S2′, S1′, S1, S2 and S3 sites respectively [34] as seen in procathepsins B, K, L and Caricain [35–37]. The proregion hydrolysis is avoided by its positioning in the reverse direction in regard to the substrate peptide [38].

3.3. Ribonucleotide UDP

During the process of structure refinement, an unaccounted electron density was observed close to the helix α4 and strand β3 and the proregion residues Asp41, Arg43 and Phe45 in all four chains of the asymmetric unit. After careful analysis this electron density was identified to a ribonucleotide and the electron density contour at carbon C2′ of the ribonucleotide pentose ring established that it is a ribose. The two pyrimidine ribonucleotide diphosphate, cytosine and uracil, can be modeled within this electron density and neither the monophosphate nor the triphosphate ribonucleotide satisfy the density map as well as the diphosphate. Analysis of the interactions between the ribonucleotide pyrimidine ring and Xylellain side chains suggests that the C4 oxygen of uracil can satisfy a hydrogen bond with the nitrogen of Tyr184 backbone, while the cytosine C4 nitrogen will not form such a bond. From these observations we propose that the nucleotide is a uridine diphosphate (UDP). An electron density omit map for the UDP is shown in Fig. 3. The UDP binding pocket is formed by Asp41, Arg43, Asp44, Phe45 and Lys131, Lys135, Tyr184. The first four from the proregion, Lys131 and Lys135 from helix α4 and Tyr184 from strand β3 (Fig. 3). The UDP pyrimidine ring is stacked between Phe45 and Tyr184 aromatic rings, hydrogen bonds are observed between the UDP O2 and O4 and the main chain nitrogen of Phe45 and Tyr184, respectively, and also between the N3 with

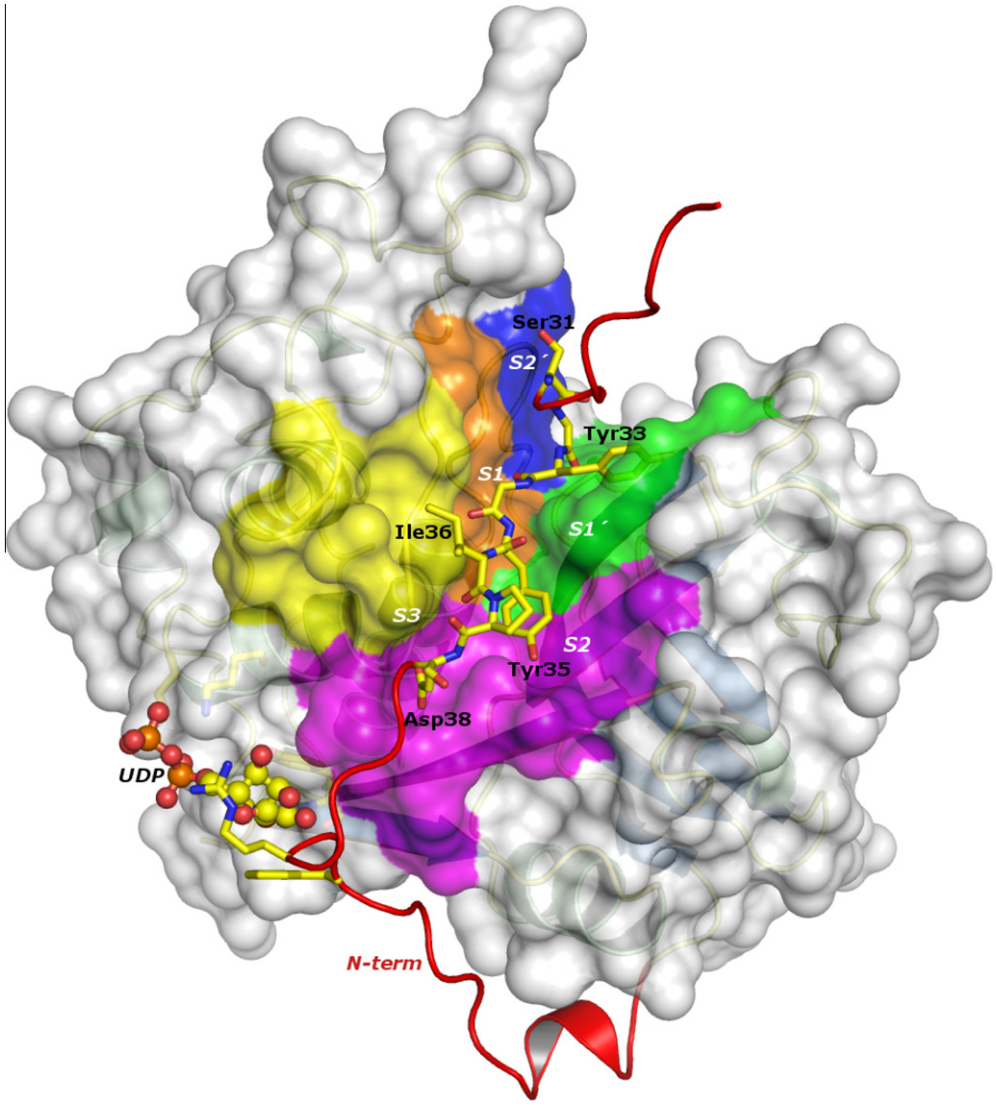

Fig. 2. Representation of the surface of Xylellain, showing the interaction between the proregion (red cartoon and yellow sticks) and the proregion-binding sites, S1′ (green), S2′ (blue), S1 (orange), S2 (magenta) and S3 (yellow). Stick representations show residues complementary to the substrate-binding site.

the main chain oxygen of Tyr184. The negative charged phosphate groups of UDP are accommodated by Lys131 and Lys135 from helix α4 and Arg43 from the proregion (Fig. 3).

The role of UDP in Xylellain is an intriguing topic. To our knowledge this is the first time a ribonucleotide is found in a protease. In an attempt to address its role, residues Arg43 and Phe45 were substituted for Ala by site-directed mutagenesis, generating the Xylellain Arg43Ala, Phe45Ala and the double mutant Arg43Ala/Phe45Ala and their kinetic parameters were compared with the native Xylellain (Table 2).

Comparison of the kinetic results indicate a more significant alteration of the k_m values from the native Xylellain for the double mutant Arg43Ala/Phe45Ala = 28(1) μM and the single mutant Phe45Ala = 124,6(9) μM, than the observed effect of the mutations on the k_{cat}/k_m values, that remain mostly constant and within the experimental error (Table 2).

4. Discussion

4.1. Structure of Xylellain

Xylellain shares a common fold with other cystein proteases. The 39 amino acid residues representing Xylellain propeptide is analogous to other cystein proteases, like catepsin B (3PBH), K (7PCK) and L (1BY8) [35,36] although shorter. Cystein proteases proregion form extensive contacts with a loop and a β-strand region on the protein surface, forming a structure called "Proregion Binding Loop" (PBL) [39]. These proregions are accommodated in the active site cleft mimicking the substrate interactions with the catalytic residues, however, self-cleavage is inhibited by its reverse orientation in relation to the substrate. The proregion can be divided in two segments (I and II). Segment I (Thr23 to Arg28) is free of the active site and could be a cellular signal sequence, while segment II (Lys29 to Ile39) fits in the active site and is stabilized by seven hydrogen bonds (Fig. 2) and Ser21, Tyr23, Tyr25, Ile26, Asp28 interaction with S2′, S1′, S1, S2 and S3 sites (Fig. 2).

One intriguing and novel aspect of this structure is the presence of a bound UDP. The pyrimidine ring identity was determined by the UDP fitting in the electron density map. The Xylellain side chains residues interaction with the pyrimidine ring show that uracil C4 oxygen satisfies the hydrogen bond with Tyr184 nitrogen, strengthening our initial identification. Citosine C4 nitrogen would not form such a hydrogen bond.

The UDP binding pocket location, at the bent of the proregion leaving the active site cleft, decreases the flexibility of this region

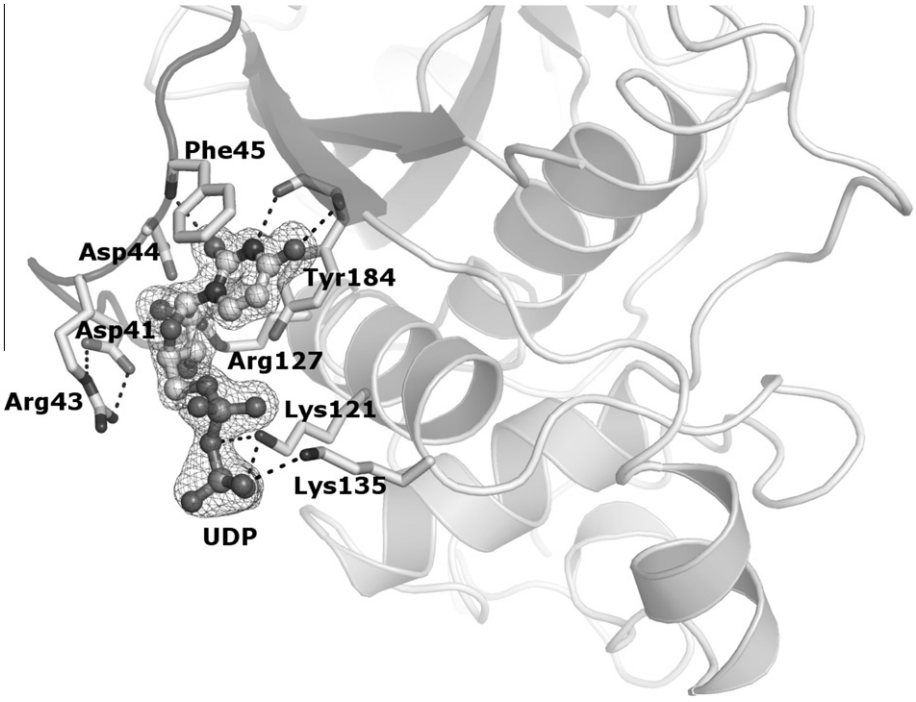

Fig. 3. UDP molecule interaction and identification. A σ-weighted 2 Fo – Fc omit electron-density map is shown contoured at 1.0σ for the area surrounding the ligand (UDP). A hydrophobic pocket is formed by residues Phe45 and Tyr184 interacting the nitrogen base of UDP. Hydrogen bonds complement the nucleotide binding pocket. Positively charged residues Arg43, Lys131 and Lys135 form a large charged surface that interacts with the negatively charged phosphates of UDP. A hydrogen-bonding network (Asp41-Arg43, Asp44-Arg141) maintains the N-terminal proregion near the protein core.

Table 2
Comparison of enzyme kinetics between native and mutant Xylellain.

	k_m (μM)	k_{cat}/k_m ($1/mM^{-1}\ s^{-1}$)
Native Xylellain	69 ± 6	0.22 ± 0.2
Mutant Arg43Ala	35 ± 4	0.12 ± 0.1
Mutant Phe45Ala	124.6 ± 9	0.33 ± 0.3
Mutant Arg43Ala/Phe45Ala	28 ± 1	0.25 ± 0.2

as revealed by the mean b-factors of 16.6 $Å^2$ of this region as compared to the overall structure of 22.8 $Å^2$. The position and the strong interactions of UDP with the proregion suggest a contribution to the N-terminal sequence fitting in the active site cleft.

The kinetic data (Table 2) revealed that mutations in the UDP binding pocket, that prevent the ribonucleotided stabilization, resulted in a strong k_m variation for the substrate, but maintain the k_{cat}/k_m values, suggesting that the UDP influences the substrate accessibility to the active site cleft not affecting catalytic efficiency (Table 2).

We hypothesize that UDP acts as a physiological regulator of the activation of Xylellain. Destabilization of this nucleotide as a result of cell signaling events would cause segment II of the proregion to lose its interaction with the cleft surface and leave the active site more exposed and accessible to the substrate. In contrast, in the presence of UDP, segment II would interact perfectly with the active site, preventing unwanted proteolysis. Our findings suggest a novel mechanism for the regulation of the activation of cysteine proteases.

4.2. Protein data bank accession code

Protein coordinates and structure factors were deposited on RCSB protein data bank under PDB code 3OIS.

Acknowledgements

The work was supported in part by the Research Grant 98/14138-2 to GO and NRL, MAOD, ARF, LMF and AG had student fellowships from the *Fundação de Amparo à Pesquisa no Estado de São Paulo* (FAPESP). We would like to thank the members of the Protein Crystallography and Structural Biology Group (IFSC-USP) and Laboratory of Molecular Biology (DGE-UFSCar) for helpful discussions in the course of this work, Dr. Susana A. Sculaccio, José A. L. da Costa, José G. Catarino and Norma B. Saes for technical help. The data collection was performed at the "*RapiData2006*" at Brookhaven National Ligth Source with Thanks to Dr. Alexei Soares for data collection and Initial data processing and phasing assistance.

References

[1] Purcell, A.H. and Hopkins, D.L. (1996) Fastidious xylem-limited bacterial plant pathogens. Annu. Rev. Phytopathol. 34, 131–151.
[2] Lambais, M.R. et al. (2000) A genomic approach to the understanding of *Xylella fastidiosa* pathogenicity. Curr. Opin. Microbiol. 3, 459–462.
[3] Koide, T. et al. (2004) DNA microarray based genome comparison of a pathogenic and a nonpathogenic strains of *Xylella fastidiosa* delineates genes important for bacterial virulence. J. Bacteriol. 186, 5442–5449.
[4] Rossetti, V. and De Negri, J.D. (1990) Clorose variegada dos citros – revisão. Laranja 11, 1–14.
[5] Hendson, M. et al. (2001) Genetic diversity of Pierce's disease and other pathotypes of *Xylella fastidiosa*. Appl. Environ. Microbiol. 67 (2), 895–903.
[6] Van Sluys, M.A. et al. (2003) Comparative analyses of the complete genome sequences of Pierce's disease and citrus variegated chlorosis strains of *Xylella fastidiosa*. J. Bacteriol. 3, 1018–1026.
[7] Monteiro, P.B. et al. (2001) Stable transformation of the *Xylella fastidiosa* citrus variegated chlorosis strain with oriC plasmids. Appl. Environ. Microbiol. 67, 2263–2269.
[8] Williams, P.H. (1980) The crucifer genetics cooperative. Plant Dis. 64, 11736–11742.
[9] Brlansky, R.H. et al. (1983) Colonization of the sharpshooter vectors, *Oncometopia nigricans* and *Homalodisca coagulata*, by xylem limited bacteria. Phytopathology 73, 530–535.

[10] Roberto, S.R. et al. (1996) Transmissão de Xylella fastidiosapelas cigarrinhas Dilobopterus costalimai. Acrogonia terminalis e Oncometopia facialis em citros Fitopatologia Brasileira 21, 517–518.
[11] De Souza, A.A. et al. (2003) Analysis of gene expression in two growth states of *Xylella fastidiosa* and its relationship with pathogenicity. Mol. Plant Microbe Interact. 16, 867–875.
[12] Simpson, A.J.G. et al. (2000) The genome sequence of the plant pathogen *Xylella fastidiosa*. Nature 406, 151–157.
[13] Nogaroto, V. et al. (2006) Recombinant expression and characterization of a *Xylella fastidiosa* cysteine protease differentially expressed in a nonpathogenic strain. FEMS Microbiol. Lett. 261, 187–193.
[14] Van Duyne, G.D., Standaert, R.F., Karplus, P.A., et al. (1993) Atomic structure of FKBP-FK506, an immunosupressant complex. J. Mol. Biol. 228, 105–124.
[15] Matsumoto, K. et al. (1999) Structural basis of inhibition of cysteine proteases by E-64 and its derivatives. Biopolymers Pept. Sci. 51, 99–107.
[16] Otwinowski, Z. and Minor, W. (1997) Processing of X-ray diffraction data collected in oscillation mode meth. Enzymology 276, 307–326.
[17] Leslie, A.G.W. (1992) Recent changes to the MOSFLM package for processing film and image data, Jt. CCCP4 ESF-EADBM. Newsl. Protein Crystallogr. 26, 27–33.
[18] Collaborative computational project number 4 (1994) Acta Crystallogr., Sec. D: Biol. Crystallogr. 50, 760–763.
[19] Matthews, B.M. (1968) The solvent content of protein crystals. J. Mol. Biol. 33, 491–497.
[20] Pauly, T.A. et al. (2003) Specificity determinants of human cathepsins revealed by crystal structures of complexes. Biochemistry 42, 3203–3213.
[21] Somoza, J.R. et al. (2002) The cristal structure of human cathepsin F and its implications for the development of novel immunomodulators. J. Mol. Biol. 322, 559–568.
[22] Gilmor, S.A. et al. (1997) Structural determinants of specificity in the cysteine protease cruzain. Protein Sci. 6, 1603–1611.
[23] Navazza, J. (1994) AMoRe: an automated package for molecular replacement. Acta Crystallogr., Sec. A: Found. Crystallogr. 50, 157–163.
[24] Vagin, A. and Teplyakov, A. (1997) MOLREP: an automated program for molecular replacement. J. Appl. Crystallogr. 30, 1022–1025.
[25] Read, R.J. (2001) Pushing the boundaries of molecular replacement with maximum likelihood. Acta Crystallogr., Sec. D: Biol. Crystallogr. 57, 1373–1382.
[26] Schneider, T.R. and Sheldrick, G.M. (2002) Substructure solution with SHELXD. Acta Crystallogr., Sec. D: Biol. Crystallogr. 58, 1772–1779.
[27] Terwilliger, T.C. and Berendzen, J. (1999) Discrimination of solvent from protein regions in native Fouriers as a means of evaluating heavy-atom solutions in the MIR and MAD methods. Acta Crystallogr., Sec. D: Biol. Crystallogr. D55, 849–861.
[28] Terwilliger, T.C. (2000) Maximum-likelihood density modification. Acta Crystallogr., Sec. D: Biol. Crystallogr. 56, 965–972.
[29] Emsley, P. and Cowtan, K. (2004) Coot: model-building tools for molecular graphics. Acta Crystallogr., Sec. D: Biol. Crystallogr. 60, 2126–2132.
[30] Laskowski, R.A. et al. (1998) Validation of protein models derived from experiment. Curr. Opin. Struct. Biol. 8, 631–639.
[31] Delano, W.L. (2002) DeLano Scientific, Palo Alto, CA, USA.
[32] Drenth, J. et al. (1968) Structure of Papain. Nature 218, 929–932.
[33] Cygler, M. and Mort, J.S. (1997) Proregion structure of members of the papain superfamily. Mode of inhibition of enzymatic activity. Biochimie 79 (11), 645–652.
[34] Schechter, I. and Berger, A. (1967) On the size of the active site in proteases. I. Papain. Biochem. Biophys. Res. Commun. 27, 157–162.
[35] Turk, D. et al. (1996) Crystal structures of human procathepsin B at 3.2 and 3.3 Å resolution reveal an interaction motif between a papain-like cysteine protease and its propeptide. FEBS Lett. 384, 211–214.
[36] LaLonde, J. et al. (1999) The crystal structure of human procathepsin K. Biochemistry 38, 862–869.
[37] Sivaraman, J. et al. (1999) Crystal structure of wild-type human procathepsin K. Protein Sci. 8, 283–290.
[38] Wiederanders, B. (2003) Structure–function relationships in class CA1 cysteine peptidase propeptides. Acta Biochim. Pol. 50, 691–713.
[39] Cygler, M. et al. (1996) Structure of ratprocathepsin B: model for inhibition of cysteine protease activity by the proregion. Structure 4 (4), 405–416.